Scientia Iranica B (2014) 21(1), 130–146

Sharif University of Technology
Scientia Iranica
Transactions B: Mechanical Engineering
www.scientiairanica.com

The effect of angle of attack on limit cycle oscillations for high-aspect-ratio wings

M. Dardel*, **K. Eskandary, M.H. Pashaei and A.H. Kiaeian Moosavi**

Department of Mechanical Engineering, Babol Nooshirvani University of Technology, Shariati Street, Babol, P.O. Box 484, Postal Code: 47148-71167, Mazandaran, Iran.

Received 12 December 2011; received in revised form 28 April 2013; accepted 9 September 2013

KEYWORDS
High aspect ratio wing;
Flap-lag and torsion;
Angle of attack;
Flutter;
Limit cycle oscillation.

Abstract. In this study, the effect of the angle of attack on the aeroelastic characteristics of high aspect ratio wing models with structural nonlinearities in unsteady subsonic aerodynamic flows is investigated. The studied wing model is a cantilever wing with flag, lag and torsion vibrations and with large deflection capability, in accordance with the Hodges-Dowell wing model. An unsteady low speed incompressible air flow is assumed to include the flow time lags. Variations of the limit cycle amplitudes and frequency with free stream velocity at different angle of attacks are carefully studied. For the considered model, the angle of attack has little effect on flutter velocity but its effect on limit cycle amplitudes and frequency is considerable. This study shows that the limit cycle amplitudes are very sensitive to variations in angles of attack.

1. Introduction

Helicopter blades and some models of aircraft have long wings with great flexibility in which nonlinear deformations have important roles to play. Great deflections of these structures are describable by structural nonlinear modeling. The presence of nonlinear structural factors with aerodynamic forces leads to unsuitable aeroelastic phenomena such as limit cycles. Therefore, careful review and understanding of these phenomena in aeroelastic systems are vital.

Modeling of long wings has been undertaken by several researchers, some of which have been mentioned here. Hodges and Dowell developed the equations of motion by two complementary methods; Hamilton's principle and the Newtonian method [1]. Tang and Dowell constructed an experimental high-aspect-ratio wing aeroelastic model with a slender body at the tip. They investigated the flutter and Limit-Cycle Oscillations (LCO) of a wing in a wind-tunnel test [2]. Tang and Dowell presented a nonlinear response analysis of a high-aspect-ratio wing aeroelastic model excited by gust loads, theoretically, and examined it in a wind-tunnel [3]. Patil et al. described a formulation for aeroelastic analysis of aircraft with high-aspect-ratio wings [4]. Malatkar explored the impact of kinematic structural nonlinearities on the dynamics of a highly deformable cantilevered wing [5]. Nichkawde presented a study of the nonlinear vibrations of metallic cantilever beams and plates subjected to transverse harmonic excitations [6]. Tang, Henry and Dowell studied the effects of a steady angle of attack on the nonlinear aeroelastic response of a delta wing model to a periodic gust [7]. Gordnier and Visbal perform relevant aeroelastic analyses for a delta wing at an angle of attack, and a computational technique capable of addressing both complex nonlinear aerodynamics and nonlinear structural features is presented [8]. Tang and Dowell presented a paper built on previous work concerned with the development of a comprehensive

*. *Corresponding author.*
E-mail addresses: dardel@nit.ac.ir (M. Dardel); keivan.eskandary yahoo.com (K. Eskandary); mpashaei nit.ac.ir (M.H. Pashaei); a_kmoosavi yahoo.com (A.H. Kiaeian Moosavi)

velocity sensitivity model for continuous scanning laser vibrometry [9]. Soltani et al. [10] have examined the flow field over a swept wing under various conditions. Ghadimi et al. [11] investigated the thermal flutter characteristics of an imperfect cantilever plate under aerodynamic loads. Davari et al. [12] studied the effects of various wings on the tail flow field by measuring the tail pressure distribution. Dardel and Bakhtiari-nejad [13] presented a static output feedback controller for aeroelastic control of a cantilevered rectangular wing in low subsonic flow. Jian and Jinwu considered the nonlinear aeroelastic response of high-aspect-ratio flexible wings [14]. They investigated the dynamic stall in accordance with the ONERA wing model and investigated the effect of aerodynamics drag on flutter and limit cycle amplitudes. Qiang et al. investigated aeroelastic modeling and calculation for high aspect ratio composite wings with different forward swept angles and skin ply orientation [15]. Gordnier et al. developed a high-order (up to 6th order) Navier-Stokes solver coupled with a structural solver that decomposes the equations of three-dimensional elasticity into cross-sectional (small-deformation and spanwise), large-deformation analyses for slender wings [16]. The resulting high-fidelity aeroelastic solver is applied to the investigation of rigid, moderately flexible and highly flexible rectangular wings undergoing a pure plunging motion. Xie et al. developed a rapid and efficient method for static aeroelastic analysis of a flexible slender wing when considering structural geometric nonlinearity [17]. A non-planar vortex lattice method herein is used to compute the non-planar aerodynamics of flexible wings with large deformation. The finite element method is introduced for structural nonlinear statics analysis.

In this work, the aeroelastic behavior of a Hodges-Dowell wing model with an incompressible unsteady aerodynamic model is investigated. A brief description of the Dowell-Hodges beam is given here. The theory is intended for application to long, straight, slender, homogeneous, isotropic beams with moderate displacements, and is accurate to second order, based on the restriction that squares of bending slopes, twist t/L, and c/L, are small with respect to unity. Radial non-uniformities (mass, stiffness, twist, etc.), chordwise offsets of the mass centroid and tension axes from the elastic axis, and the warp of the cross section are included. Other more specialized details are not considered, such as blade root feathering flexibility, torque offset, blade sweep, and curvature, nor are configurations considered in which the feathering bearing is replaced with a torsionally flexible strap [1]. In incompressible unsteady aerodynamic models the effects of wakes, compressibility and viscosity are ignored. Determination of flutter and divergence velocities and clarification of limit cycle amplitudes are investigated in the current study. Effects of changing mass ratio and the distance between the elastic axis and center of mass and other parameters, are carefully examined in aeroelastic properties. This study is done for different models of wing section to evaluate the influence of mass and inertia effects on limit cycle amplitude and flutter velocity. The effects of structural damping are considered in structural modeling. The effect of initial angle of attack on limit cycle amplitude is specified.

2. Aeroelastic equations

2.1. Structural equations of motions

In this section, a brief description of structural equations of motion of a wing model, based on the Hodges-Dowell wing model, is presented. A Hodges-Dowell wing model presents double bending and torsional vibrations. Hodges-Dowell wing models are second order equations which are valid for long, straight and thin homogeneous isotropic beams. In this study, the wing cross-section is without twist and initial warping. In this study, the wing elastic and center of mass axis are not coincided, and structural damping is included in the equations of motions.

The considered wing model is a cantilevered wing model with bending displacements of w and ν and torsion of θ, which are shown in Figure 1. The flap deflection is denoted by w, positive downward direction; lag deflection is denoted by ν, positive stream-wise direction; and pitch angle, θ, is positive nose up. A sketch of the wing section is shown in Figure 2, where c is the chord, b is the semi-chord length, $a_h b$ is the distance from the wing section mid-chord to the elastic axis, and $x_a b$ is the distance from the elastic axis to the center of mass. The length of the wing is L .

Hodges-Dowell equations of motion for a uniform elastic wing, ignoring the wing section warping, are as follows [18]:

$$EI_1 w^{(4)} + (EI_2 - EI_1)(\theta\nu'')'' + m\ddot{w} - m x_a b\ddot{\theta} + C_w w = \frac{dF_w}{dx}, \tag{1}$$

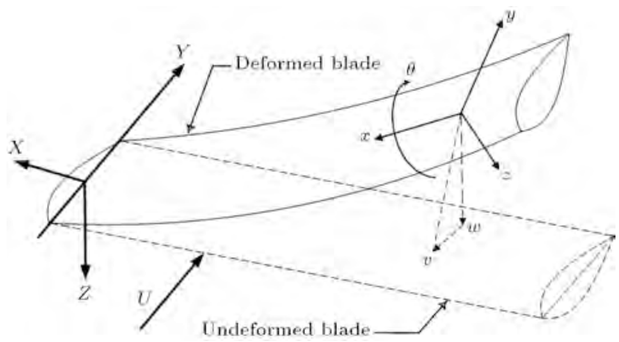

Figure 1. Flexible deflected wing.

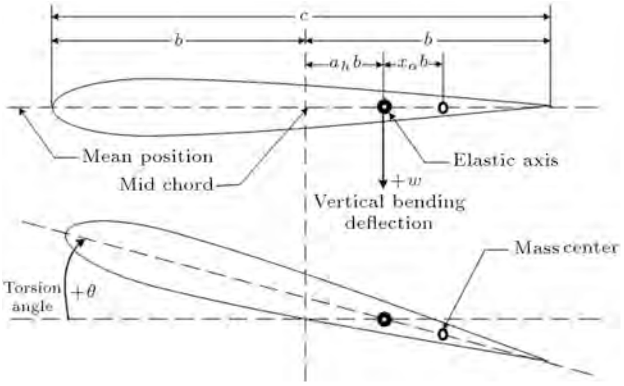

Figure 2. Schematic figure of the wing section.

$$-GJ\theta'' + (EI_2 - EI_1)w''\nu'' + mr_1^2\theta - mx_a bw + C_\theta\dot{\theta} = \frac{dM_x}{dx}, \quad (2)$$

$$EI_2\nu^{(40)} + (EI_2 - EI_1)(\theta w'')'' + m\ddot{\nu} + C_\nu\dot{\nu} = \frac{dF_\nu}{dx}, \quad (3)$$

where m, r_a, EI_1, EI_2, GJ, C_w, C_θ and C_ν are mass per unit length of the wing, radius of gyration about mass center, chord-wise and span-wise bending stiffness, torsional stiffness, respectively. $dF_w/dx, dM_x/dx$, and dF_ν/dx are aerodynamic forces and moments.

2.2. Unsteady aerodynamics model

According to work presented in [2,3,7], aerodynamic forces and moments for unsteady aerodynamics models are as follows:

$$dF_w = dL + \theta_0 dD, \quad (4)$$

$$dM_x = dM_{xf}, \quad (5)$$

$$dF_\nu = -dD + \theta_0 dL, \quad (6)$$

where θ_0, $L(t)$, $M(t)$, and $D(t)$ are a constant angle of attack, aerodynamic lift, moment and drag, respectively. Aerodynamic forces on the fixed wing model in a flow, with free flow speed, U, and according to Figure 1, are as follows [19]:

$$L(\tau) = -\rho\pi U^2\{(w'' - a_h b\theta'' + b\theta') + 2\Big[b\theta(0) = h'(0) + \left(\frac{1}{2} - a_h\right) b\theta'(0)\Big]\phi(\tau) + 2\int_0^r \phi(\tau-\sigma)[b\theta'(\sigma) + h''(\sigma)\left(\frac{1}{2} - a_h\right) b\theta'(\sigma)]d\sigma\}, \quad (7)$$

$$M(\tau) = 2\rho\pi U^2\left(\frac{1}{2} + a_h\right)\Big\{\Big[b\theta(0) + h'(0) + \left(\frac{1}{2} - a_h\right) b\theta'(0)\Big]\phi(\tau) + \int_0^r \theta(\tau-\sigma)\Big[b\theta'(\sigma) + h''(\sigma) + \left(\frac{1}{2} - a_h\right) d\theta'(\sigma)\Big]d\sigma\Big\} + \rho\pi U^2 a_h b(w'' - a_h b\theta'') - \left(\frac{1}{2} - a_h\right)\rho\pi b^2U^2\theta' - \frac{\rho\pi b^2U^2}{8}\theta''. \quad (8)$$

In these terms, all derivatives signed by ($'$) are based on dimensionless time, τ, as $\tau = Ut/b$. Wagner's function (τ) shows the flow is unsteady and is given by:

$$\phi(\tau) = 1 - \psi_1 e^{-\epsilon_1 t} - \psi_2 e^{-\epsilon_2 t}, \quad (9)$$

where $\psi_1 = 0.165$, $\varepsilon_1 = 0.041$, $\psi_1 = 0.355$, and $\varepsilon_2 = 0.32$ [8]. By inserting Eq. (9) into Eqs. (7) and (8) and using the integrating by parts, lift force $L(\tau)$ and moment $M(\tau)$ will be as follows:

$$L(\tau) = \rho\pi U^2\{w'' - a_h b\alpha + [1 + (1-2a_h)\phi(0)]\theta' + 2\phi(0)w' + 2b[\phi(0) + (0.5 - a_h)\phi'(0)]\theta(\tau) + 2\phi'(0)w(\tau) + 2b\psi_1\epsilon_1[1 - (0.5 - a_h)\epsilon_1]w_1 + 2b\psi_2\epsilon_2[1 - (0.5 - a_h)\epsilon_2]w_2 - 2\psi_2\epsilon_1^2 w_3 - 2\psi_2\epsilon_2^2 w_4 - b(1 - 2a_h)\phi'(\tau)\theta(0) - 2\phi'(\tau)w(0)]\}, \quad (10)$$

$$M(\tau) = \rho\pi U^2 b\Big\{a_h w'' - b\left(\frac{1}{8} + a_h^2\right)\theta'' + (1 + 2a_h)\phi(0)w' + (1 + 2a_h)\phi(0)w + b(0.5 - a_h)[(1 + 2a_h)\phi(0) - 1]\theta' + b(1 + 2a_h)\left[\phi(0) + (0.5 - a_h)\phi'(0)\right]\theta + b(1 + 2a_h)\psi_1\epsilon_1\Big[1 - (0.5 - a_h)\epsilon_1\Big]w_1 - (1 + 2a_h)\psi_1\epsilon_1^2 w_2 + b(1 + 2a_h)\psi_2\epsilon_2\Big[1 - (0.5 - a_h)_2\Big]w_2 - (1 + 2a_h)\psi_2\epsilon_2^2 w_4 - (1 + 2a_h)\phi'(\tau)w(0) - b(0.5 - 2a_h^2)\phi'(\tau)\theta(0)\Big\}, \quad (11)$$

which, in accordance with the definitions given by Lee et al [20], w_1, w_2 w_3 and w_4 variables are defined as follows:

$$w_1 = \int_0^\tau e^{-\epsilon_1(\tau-\sigma)}\theta(\sigma)d\sigma, \quad w_2 = \int_0^\tau e^{-\epsilon_2(\tau-\sigma)}\theta(\sigma)d\sigma,$$

$$w_3 = \int_0^\tau e^{-\epsilon_1(\tau-\sigma)}w(\sigma)d\sigma, \quad w_4 = \int_0^\tau e^{-\epsilon_2(\tau-\sigma)}w(\sigma)d\sigma. \tag{12}$$

These variables have been defined because of existing integral terms of the aerodynamics model (unsteady part of the flow). The aerodynamics center of and the distance between the elastic axis and the wing mid-chord of x_f are defined by:

$$e = \frac{x_f}{c} - \frac{1}{4}, \quad x_f = \frac{b}{2} + a_h b. \tag{13}$$

In addition, by ignoring drag force, we can write:

$$dD = 0. \tag{14}$$

2.3. Discretizing aeroelastic equations

By substituting aerodynamic forces and moments, in accordance with Eqs. (7) and (8) in the structural equations of motion (Eqs. (1)-(3)), complete aeroelastic equations will be obtained. These equations can be discretized according to the assumed mode and Galerkin's method. In these methods, the w, ν and θ displacements are explained in terms of multiplying generalized coordinate and mode shapes, which satisfy geometric boundary conditions. Then, by substituting these displacements in equations of motion, multiplying each equation with an admissible mode function and integrating along the whole area of the wing, the equations of motion will be discretized. Hence the flap, lag and torsion displacements can be described as follows:

$$w(x,t) = \sum W_i(t)\psi_i(x), \quad \theta(x,t) = \sum \theta_i(t)\phi_i(x),$$

$$\nu(x,t) = \sum V_i(t)a_i(x),$$

$$w_1 = \sum w_{1j}(\tau)\phi_j(x), \quad w_2 = \sum w_{2j}(\tau)\phi_j(x),$$

$$w_3 = \sum w_{3j}(\tau)\psi_i(x), \quad w_4 = \sum w_{4j}(\tau)\psi_i(x), \tag{15}$$

where:

$$w_{1j} = \int_0^\tau e^{-\epsilon_1(\tau-\sigma)}\theta_j(\sigma)d\sigma, \quad w_{2j} \int_0^\tau e^{-\epsilon_2(\tau-\sigma)}\theta_j(\sigma)d\sigma,$$

$$w_{3j} = \int_0^\tau e^{-\epsilon_1(\tau-\sigma)}\zeta_j(\sigma)d\sigma, \quad w_{4j} = \int_0^\tau e^{\epsilon_2(\tau-\sigma)}\zeta_j(\sigma)d\sigma, \tag{16}$$

where $W_i(t)$, $\theta_i(t)$ and $V_i(t)$ are generalized coordinates, and $\psi_i(x)$, $\phi_i(x)$ and $a_i(x)$ are mode shapes that satisfy geometric boundary conditions. Appropriate mode shapes for description of the displacements of w, v and θ are obtained from the beams and rod with equivalent boundary conditions to the wing model. This aeroelastic model has flap, lag and torsion motions. Flag and lag motions are transverse displacements. According to the Rayleigh-Ritz method, displacements can be written in terms of generalized coordinates and assumed mode functions. These mode functions must satisfy geometric boundary conditions. Accordingly, flap and lag displacements are written in terms of mode functions of the Euler-Bernoulli cantilever beam, and torsion displacement is expressed in terms of the fixed-free mode function of the shaft or rod. These mode shapes are as follows:

For bending modes:

$$\psi_n = \sin\beta_n\frac{x}{L} - \sinh\beta_n\frac{x}{L} + a_n\left(\cos\beta_n\frac{x}{L} - \cosh\beta_n\frac{x}{L}\right), \tag{17}$$

that:

$$\beta_n = 1.8751, 4.6941, 7.8547, 10.9955, 10.9955 + \pi, \cdots$$

$$a_n = (\cos\beta_n - \cosh\beta_n)/(\sin\beta_n = \sinh\beta_n),$$

and, for torsional modes:

$$\phi_n = \sin\left(\frac{2n-1}{2}\pi\frac{x}{L}\right). \tag{18}$$

The following non-dimensional quantities are introduced:

$$\tau = \frac{U_\infty t}{b}, \quad \zeta = \frac{w}{b}, \quad \eta = \frac{\nu}{b},$$

$$r_a = \sqrt{\frac{I_a}{mb^2}}, \quad \mu = \frac{m}{\rho\pi b^2}, \quad U^* = \frac{U}{b\omega_a},$$

$$\omega_\alpha = \sqrt{\frac{GJ}{I_\theta L^2}\frac{\int_0^1 \left(\overset{-\prime\prime}{\phi_1}\right)^2 dx^-}{\int_0^1 \left(\overset{-\prime\prime}{\phi_1}\right)^2 dx^-}}$$

$$\omega_\zeta = \sqrt{\frac{EI_1}{I_{mL^4}}\frac{\int_0^1 \left(\overset{-\prime\prime}{\psi_1}\right)^2 dx^-}{\int_0^1 \left(\overset{-}{\psi_1}\right)^2 dx^-}},$$

$$\omega_\eta = \sqrt{\frac{EI_1}{I_{mL^4}}\frac{\int_0^1 \left(\overset{-\prime\prime}{a_1}\right)^2 dx^-}{\int_0^1 \left(\overset{-}{a_1}\right)^2 dx^-}},$$

$$\omega_1^* = \frac{\omega_\zeta}{\omega_a}, \quad \omega_2^* = \frac{\omega_\eta}{\omega_a}, \quad \xi = \frac{x}{L}, \tag{19}$$

where ζ and η are dimensionless flap and lag deflections; ω_ζ, ω_η and ω_a are the first natural frequencies of uncoupled flap, lag and pitching modes; U^*, ω_i^* and μ are dimensionless velocity, bending to torsion frequency ratios and mass ratio, respectively, and ζ is dimensionless coordinate along the span of the wing. These dimensionless parameters are defined in order to select the necessary parameters, in accordance with the values given in [9], to validate the presented model, in accordance with the flutter velocities in this reference.

By combining structural equations (Eqs. (1)-(3)) with aerodynamic equations (Eqs. (7)-(8)), expressing displacement variables according to Eq. (15), applying Galerkin's method and using dimensionless parameters given in Eq. (19), the original partial differential equations are converted to the following ordinary differential equations:

$$\begin{bmatrix} M_{\zeta\zeta} & M_{\zeta\theta} & M_{\zeta\eta} \\ M_{\theta\zeta} & M_{\theta\theta} & M_{\theta_\eta} \\ M_{\eta\zeta} & M_{\eta\theta} & M_{\eta\eta} \end{bmatrix} \begin{Bmatrix} \ddot{\zeta} \\ \ddot{\theta} \\ \ddot{\eta} \end{Bmatrix} + \begin{bmatrix} C_{\zeta\zeta} & C_{\zeta\theta} & C_{\zeta\eta} \\ C_{\theta\zeta} & C_{\theta\theta} & C_{\theta_\eta} \\ C_{\eta\zeta} & C_{\eta\theta} & C_{\eta\eta} \end{bmatrix}$$

$$\times \begin{Bmatrix} \zeta \\ \theta \\ \eta \end{Bmatrix} + \begin{bmatrix} K_{\zeta\zeta} & K_{\zeta\theta} & K_{\zeta\eta} \\ K_{\theta\zeta} & K_{\theta\theta} & K_{\theta_\eta} \\ K_{\eta\zeta} & K_{\eta\theta} & K_{\eta\eta} \end{bmatrix} \begin{Bmatrix} \zeta \\ \theta \\ \eta \end{Bmatrix}$$

$$+ \begin{bmatrix} K_{\zeta 1} & K_{\zeta 2} & K_{\zeta 3} & K_{\zeta 4} \\ K_{\theta 1} & K_{\theta 2} & K_{\theta 3} & K_{\theta 4} \\ K_{\eta 1} & K_{\eta 2} & K_{\eta 3} & K_{\eta 4} \end{bmatrix} \begin{Bmatrix} w_{1i} \\ w_{2i} \\ w_{3i} \\ w_{4i} \end{Bmatrix} = \begin{Bmatrix} F_{N\zeta} \\ F_{N\theta} \\ F_{N\eta} \end{Bmatrix}. \tag{20}$$

Elements of each matrix and nonlinear terms in Eq. (20) are introduced in Appendix A.

According to the definition presented in Eq. (12), time derivatives of variables w_1, w_2, w_3 and w_4 are defined as follows:

$$\frac{d}{d\tau}\begin{Bmatrix} w_{1i} \\ w_{2i} \\ w_{3i} \\ w_{4i} \end{Bmatrix} = \begin{Bmatrix} \theta_j \\ \theta_j \\ \zeta_j \\ \zeta_j \end{Bmatrix} - \begin{bmatrix} \epsilon_1 & 0 & 0 & 0 \\ 0 & \epsilon_2 & 0 & 0 \\ 0 & 0 & \epsilon_1 & 0 \\ 0 & 0 & 0 & \epsilon_2 \end{bmatrix} \begin{Bmatrix} w_{1i} \\ w_{2i} \\ w_{3i} \\ w_{4i} \end{Bmatrix}. \tag{21}$$

Aeroelastic equations can be obtained by combining Eqs. (20) and (21). These equations can be written briefly as follows:

$$[M_{eq}]\{\ddot{q}\} + [C_{eq}]\{\dot{q}\} + [K_{eq}]\{q\} + [K_{\text{Lag}}]\{w_{\text{Lag}}\} = \{F_N\},$$

$$\left\{\frac{dw_{\text{Lag}}}{d\tau}\right\} = \{u\} - [K_\epsilon]\{w_{\text{Lag}}\}, \tag{22}$$

where $[M_{eq}]$, $[C_{eq}]$ and $[K_{eq}]$ are mass, damping and stiffness matrices and $\{F_N\}$ is a vector of structural nonlinearity. $[K_{\text{Lag}}]$ and $[K_\epsilon]$ show the effect of aerodynamics lag due to unsteadiness of flow. The vectors, $\{q\}$ and $\{w_{\text{Lag}}\}$, are defined as $\{\zeta^T \theta^T \eta^T\}^T$ and $\{w_{\text{Lag}}\} = \{w_{1i}^T\ w_{2i}^T\ w_{3i}^T\ w_{4i}^T\}^T$, respectively.

Now, after presenting all aeroelastic equations, the validity and results obtained from these equations will be examined.

3. Aeroelastic results

In this section, the aeroelastic results of the presented wing model for different cases will be studied. For this purpose, at first, wing structural and aerodynamics parameters will be selected. Wing sections and flight parameters are shown in Table 1. These parameters

Table 1. Wing model data.

Wing specification	**Values**
Span (L)	0.6299 (m)
Chord (c)	0.1018 (m)
Dimensionless distance from wing section mid-chord to elastic axis (a_h)	−0.3
Dimensionless distance from elastic axis to center of mass (x_a)	−0.22
Flap structural modal damping (C_w)	0.02
Chord-wise structural modal damping (C_v)	0.025
Torsional structural modal damping (C_θ)	0.031
Mass ratio (μ)	48
Radius of gyration about elastic axis (r_α)	0.558
Natural frequencies in flap bending (ω_ζ)	$26 \times \pi \left(\frac{\text{rad}}{\text{s}}\right)$
Natural frequencies in chord-wise bending (ω_η)	$172.6 \times \pi \left(\frac{\text{rad}}{\text{s}}\right)$
Natural frequencies in torsion (ω_α)	$210 \times \pi \left(\frac{\text{rad}}{\text{s}}\right)$
Flight conditions	
Density of air (ρ)	$1.1 \left(\frac{\text{kg}}{\text{m}^3}\right)$

are selected compatible with parameters presented in [2,21]. These parameters are not selected accurately, according to parameters given in these references, since, in [2], the parameters are for a wing which represents stall phenomenon, and parameters given in [21] are for a simple wing model with plunge and pitch motions, with low speed and incompressible, irrotational aerodynamic flow. Hence, combinations of the parameters given by these references are given in Table 1.

3.1. Eigenvalue solution of the linear aeroelastic system at zero angle of attack

At first, the eignevalue solution of the linear aeroelastic system at zero angle of attack, which determines the stability of the linear part of the system, will be studied. For this purpose, considering the derivative of all variables in Eq. (22) equal to zero, the equilibrium point of the equation of motion will be determined. Then, by linearization of the nonlinear terms, an equivalent linear system around the equilibrium point will be obtained, and from this equivalent linear system, eigenvalue analysis is carried out.

Changes of eigenvalues of the linear aeroelastic equation with free stream velocity have been shown in Figures 3-5. The damping and frequency of eigenvalues are given by the real and imaginary parts of eigenvalues, λ, of the linear system. Different combinations of mode shapes are selected and the convergences of the eigenvalue solution are studied. For these figures, the number of the mode functions for flap, lag and torsion displacements are 4, 2 and 2. By increasing the number of mode shapes above these mentioned mode numbers, minor changes will occur in the predictions. A sample convergence of the solution, based on the number of the mode shapes, will be presented in the next section.

As seen in Figure 3, by increasing the free stream velocity, one of the branches of the real part of the eigenvalues of the linear system will change its sign and become positive. In this case, the initially stable system becomes unstable. In flutter velocity, a branch of eigenvalues has an intersection with the real axis. For this intersection, the real part of the corresponding eigenvalue is zero. When the flutter velocity is $U_F = 102.271$ m/s (Figure 4), by increasing free stream velocity, at first, all branches move to the left side of the imaginary axis, which means more stability of the system, but, at a velocity of 83.75 m/s, two of these branches move towards the imaginary axis, which means that the system tends to be unstable.

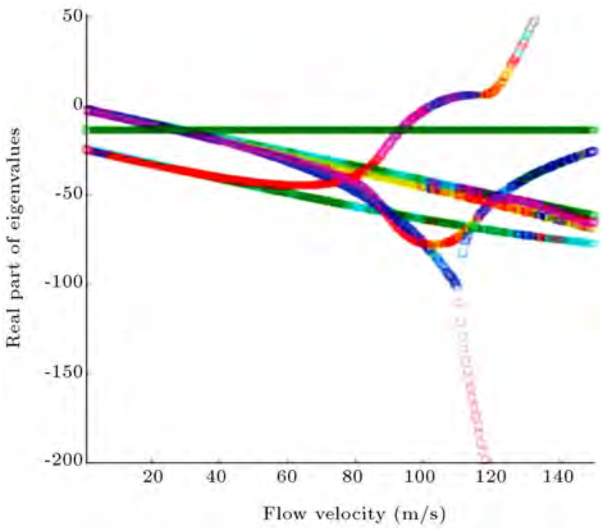

Figure 3. Real part (damping) of eigenvalues of the linearized aeroelastic system vs. free stream velocity, case 1.

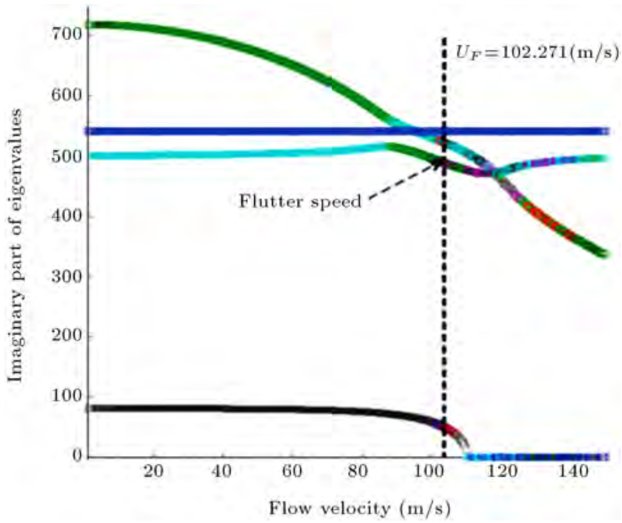

Figure 4. Imaginary part (frequency) of eigenvalues of the linearized aeroelastic system vs. free stream velocity, case 1.

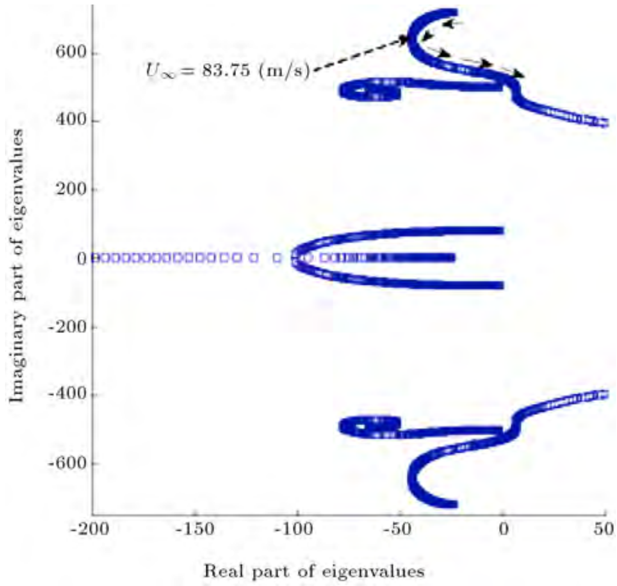

Figure 5. Imaginary part (frequeny) vs. real part (damping) of the eigenvalues of the linearized aeroelastic system, case 1.

After getting the branches to the imaginary boundaries and passing them, the linear system became unstable. Moreover, from Figure 5, it is clear that the two branches of eigenvalues approach each other gradually and near flutter velocity, they have less distance from each other, which shows the bending-torsion flutter mode. From Figure 4, the second mode of flap bending with the first mode of torsion is the reason for the flutter. In this type of flutter, increasing the free stream velocity causes the bending frequency to increase and the torsion frequency to decrease. Once these frequencies become nearly equal, a flutter of coupled bending-torsion occurs, whose effect is similar to the internal resonance phenomenon, and between these branches, an internal resonance occurs. Flutter is a linear dynamics phenomenon, in which the aerodynamics force dominates the dynamics inertial forces. In flutter, unstable eigenvalues are in complex conjugate form, and the amplitude of vibration gradually increases with time. But, if there is nonlinearity in the system, the counter effects of unstable eigenvalues after flutter velocity with nonlinear structural terms, lead to a nonlinear vibration phenomenon, such as limit cycle. Limit cycle oscillation is a vibration with limited amplitude.

Divergence is static instability, in which aerodynamic forces dominate structural force (wing stiffness) without consideration of inertia forces. Explained mathematically, this is instability with pure positive real eigenvalue (eigenvalue without an oscillatory imaginary part). For divergence of the wing, it is necessary for eigenvalues of a linearized system to go to the right half of the s-plane along the horizontal axis, without having an imaginary part. From Figure 5, some eigenvalues of the considered linearized aeroelastic system lie on the negative horizontal axis. These real negative eigenvalues are due to the lag in aerodynamics force, i.e. dynamics of the aerodynamic forces through w_{Lag} (Eq. (22)). Also, by varying velocity, two branches of eigenvalues, according to Figure 5, intersect and bifurcate, and one branch moves along the negative real axis, and another moves towards the positive real axis. For occurring divergent instability, it is necessary to increase the free stream velocity. For the case considered here, the required free stream velocity for divergent instability is beyond the applicability of the considered aerodynamics model. Hence, the free stream velocity is limited to the domain shown in these figures. As shown in Figure 5, the eigenvalues on real axes are on the left half plane. Similar forms of behavior are presented in [9,10].

3.2. Solution convergence study

Here, the effect of different numbers of mode shape on the convergence of the solution will be studied. This convergence study is briefly described in Figures 6-8. These figures show the displacement at the tip of the wing. As seen from these figures, there are minor changes of predictions based on the 3-2-2 and 4-2-2 number of mode shapes. Hence, selection of the 4, 2 and 2 mode shapes for flap, torsion and lag displacements are very justified.

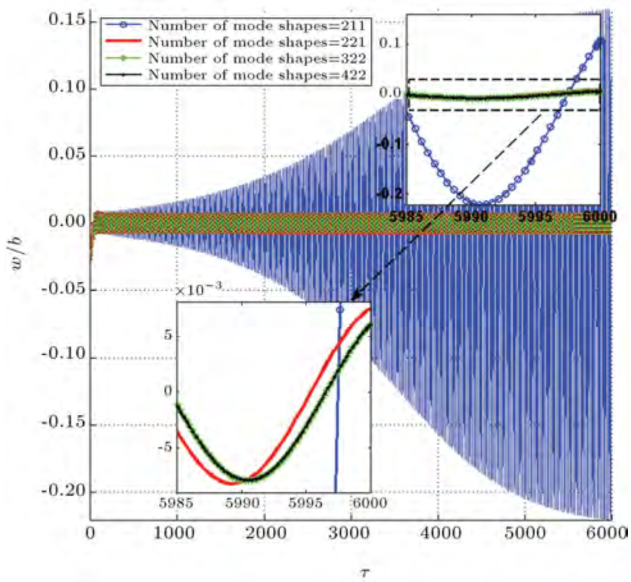

Figure 6. Flap displacement of the nonlinear aeroelastic wing model at angle of attack 1 deg in $U_\infty = 102.271$ m/s for different combinations of mode shapes (tip of the wing).

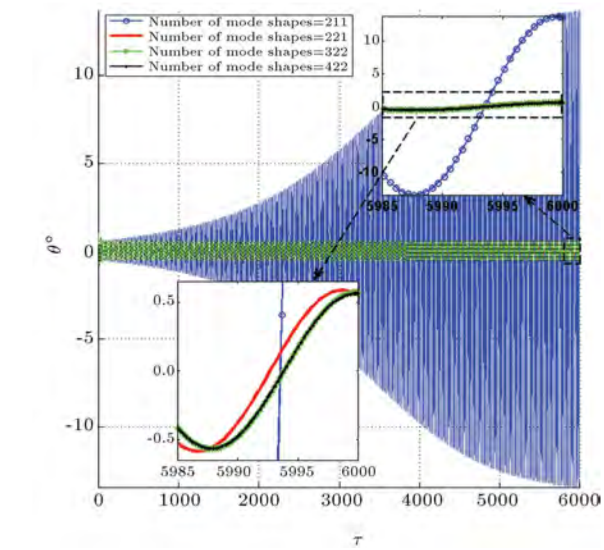

Figure 7. Torsional displacement of the nonlinear aeroelastic wing model at angle of attack 1 deg in $U_\infty = 102.271$ m/s for different combinations of mode shapes (tip of the wing).

3.3. Effect of the free stream velocity of limit cycle amplitudes

After examination of the linear stability of the aeroelastic model and selection of the correct number of mode shapes, the time response of the nonlinear aeroelastic

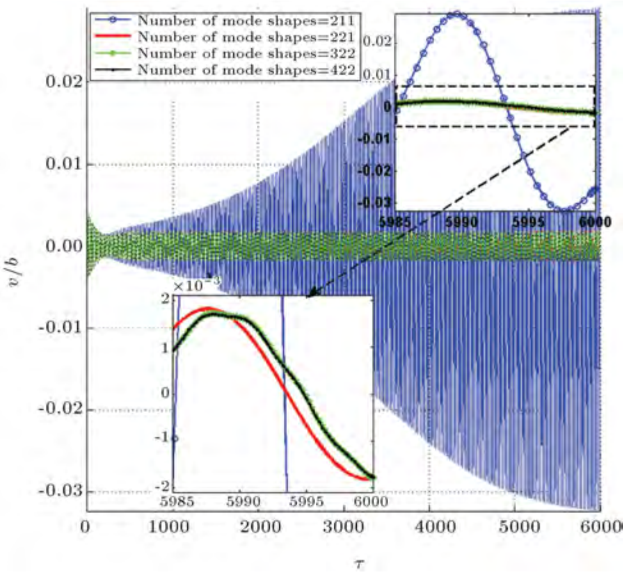

Figure 8. Lag displacement of the nonlinear aeroelastic wing model at angle of attack 1 deg in $U_\infty = 102.271$ m/s for different combinations of mode shapes (tip of the wing).

model in different velocities will be examined. The limit cycle oscillation amplitudes for two different velocities are shown in Figures 9 and 10.

As seen from Figure 9, in velocity less than the linear flutter velocity, vibration amplitudes decreases with time and finally becomes damp. In this velocity, all eigenvalues of the linear system have a negative real part, and the linear system is stable. Hence, the amplitude of the oscillation gradually moves to zero. As seen from Figure 10, by increasing the free flow velocity above the flutter boundary, limit cycle oscillations will occur. The reason is that in a velocity greater than linear flutter, the linear system has complex conjugate positive real part eigenvalues, which tend to increase the amplitude of the vibrations. In the absence of the structurally nonlinear term, the amplitude of the oscillations tends to infinity, while by increasing the amplitude of the oscillations, the nonlinear structural terms become sufficiently large and prevent further increase in the vibration amplitude. Hence, finally, the oscillation will settle down in a nonlinear absorber, which is the limit cycle, in this case.

The effects of the different free stream velocity in the time response of nonlinear aeroelastic model are shown in Figures 11-13. These displacements are shown for the tip of the wing. From Figure 13, by increasing velocity beyond linear flutter velocity, the amplitude of the tip flap displacements increases at first, and then, decreases. Similar forms of behavior are presented for torsion and lag displacements.

From Figure 12, the torsion displacement is symmetric, but the flap and lag displacements of Figures 11 and 13 are not symmetric. The flap and lag displacements have a static deformation in the direction of the flow, and the whole of the wing will oscillate in

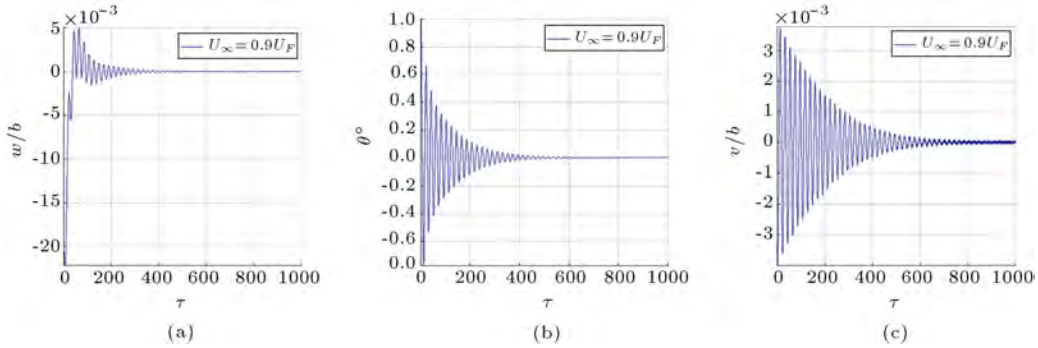

Figure 9. Wing tip (a), flap (b), torsion (c), and lag deflections in $U_\infty = 0.9U_F$ and angle of attack 1 deg.

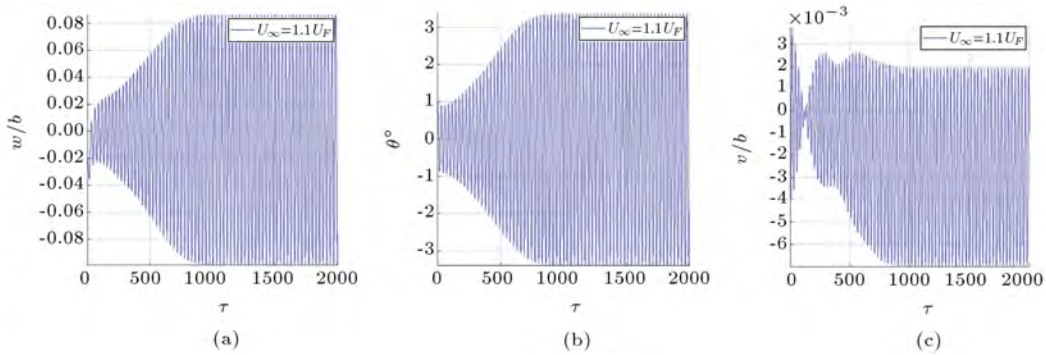

Figure 10. Wing tip (a) flap (b), torsion (c), and lag deflections in $U_\infty = 1.1U_F$ and angle of attack 1 deg.

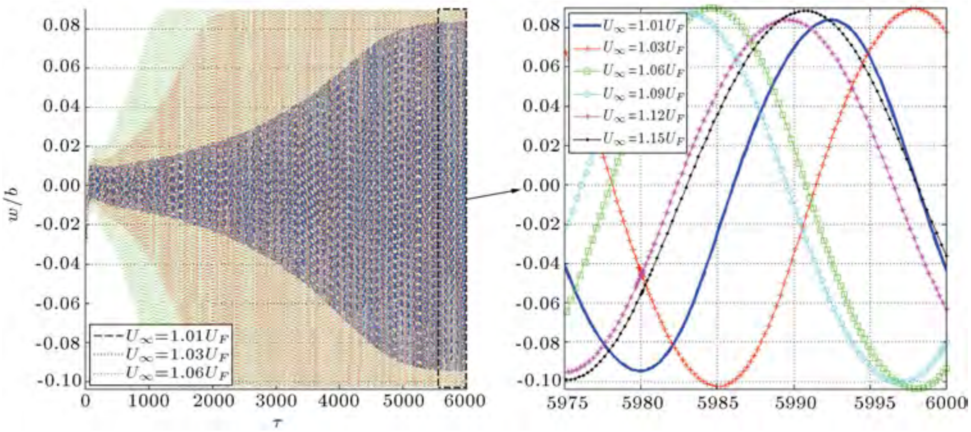

Figure 11. Flap displacement of the nonlinear aeroelastic wing model in different free stream velocity at angle of attack 1 deg.

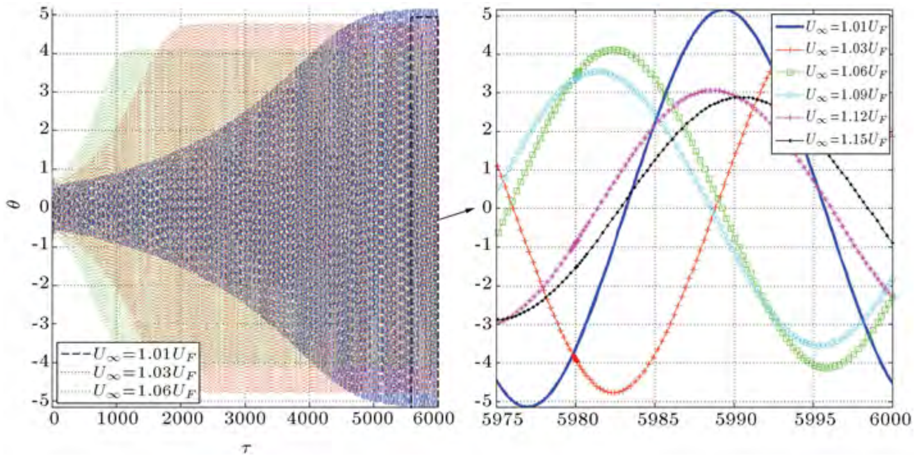

Figure 12. Torsion displacement of the nonlinear aeroelastic wing model in different free stream velocity at angle of attack 1 deg.

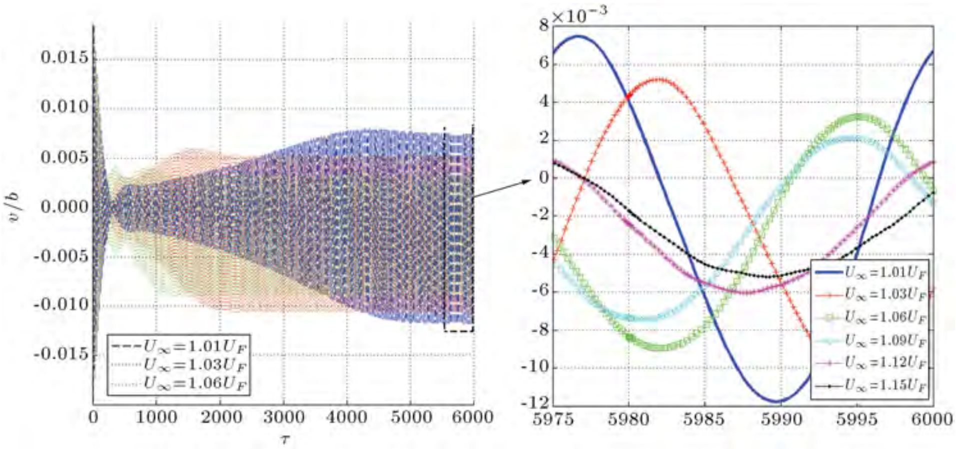

Figure 13. Lag displacement of the nonlinear aeroelastic wing model in different free stream velocity at angle of attack 1 deg.

the vicinity of this static displacement. According to these figures, in velocities greater than flutter velocity, the aerodynamics force is divided into two sections. Some parts of the aerodynamics and structural forces counteract each other without inclusion of the inertial forces and produce a static displacement of the wing. Remaining parts of the aerodynamics forces will counteract structural and inertial forces and produce oscillations around this static state. Hence, the limit cycle amplitudes decrease with increasing velocity.

The maximum amplitudes of flap, torsion and lag displacements along the span of the wing are shown in

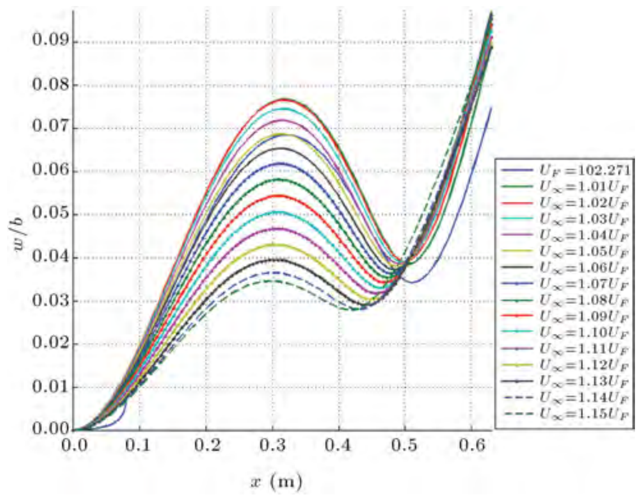

Figure 14. The flap displacement amplitude along the span of the wing for different velocities at angle of attack 1 deg.

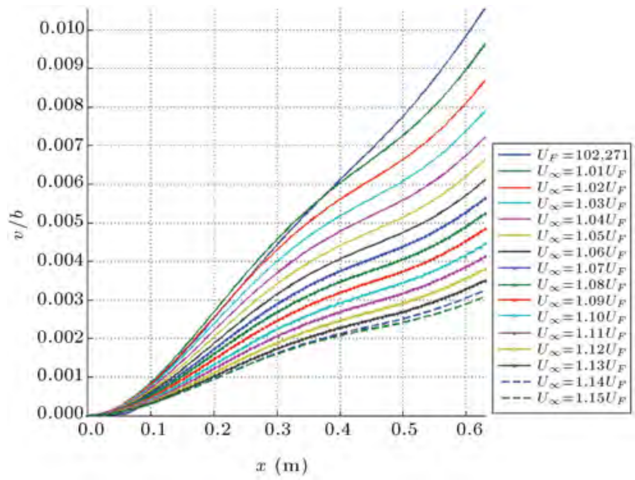

Figure 16. The lag displacement amplitude along the span of the wing for different velocities at angle of attack 1 deg.

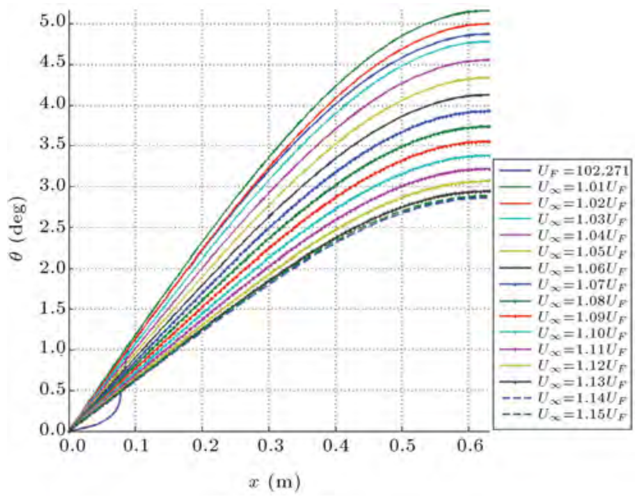

Figure 15. The torsion displacement amplitude along the span of the wing for different velocities at angle of attack 1 deg.

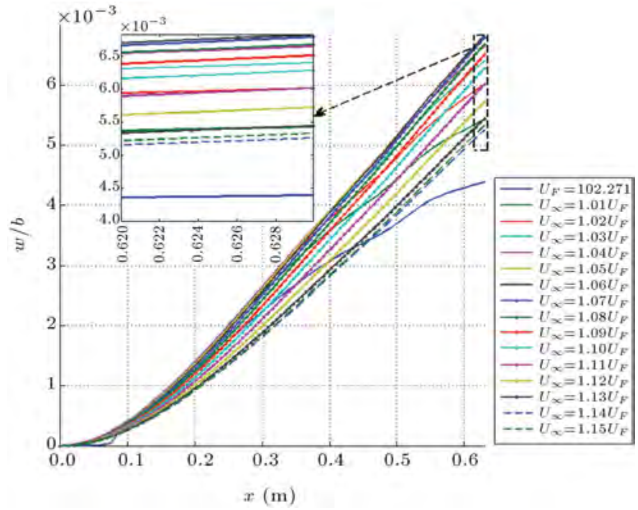

Figure 17. The flap static displacement along the span of the wing for different velocities at angle of attack 1 deg.

Figures 14-16, respectively. According to Figure 14, for velocities greater than flutter velocity, the flap displacement at the tip of the wing is nearly constant. By increasing free stream velocity up from 1.01 U_F, the torsion displacement decreases (Figure 15). For the lag displacement according to Figure 16, the maximum amplitude at the tip of the wing decreased with an increase in free stream velocity up to 1.15 U_F. At mid wing, the amplitude of the limit cycle oscillation decreased.

As shown in Figure 11, there is a certain static displacement in flap displacements. This static displacement has been shown in Figure 17 for the whole span of the wing. According to Figure 17, up to $U_\infty = 1.05 \times U_F$ by increasing velocity, static displacement amplitude increases, and by increasing free stream velocity up from 1.06 U_F, the static amplitude displacement decreases. There is a similar situation for torsion and lag static displacements, as shown in Figures 18 and 19.

Maximum limit cycle amplitudes along the wing span, at angle of attack, are shown in Figures 20-25.

According to Figures 21 and 22, in this angle of attack, by increasing free stream velocity, the lag and torsion amplitudes at the end of the wing, at first, increase and then decrease, while there are not important changes for flap amplitudes. By comparing the results presented in Figures 14-19 with Figures 20-25, it is seen that by increasing the angle of attack from to, the lag displacements at the end of the wing are increased, while flap and torsion displacement has little change.

Also, by comparing Figures 17-19 and Figures 23-25, it is seen that the static displacements of the wing increase by increasing the angles of attack.

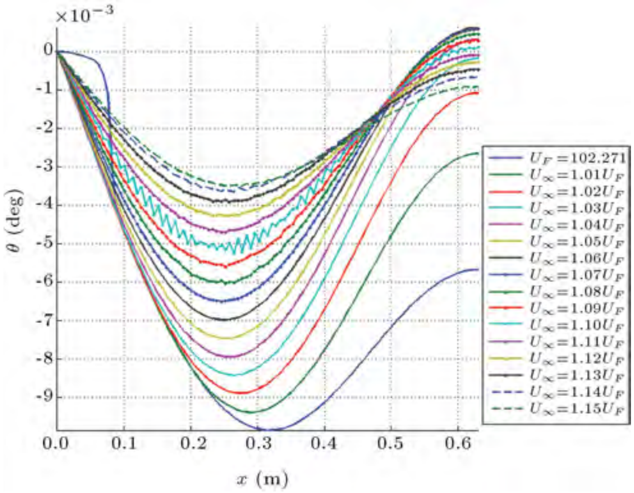

Figure 18. The torsion static displacement along the span of the wing for different velocities at angle of attack 1 deg.

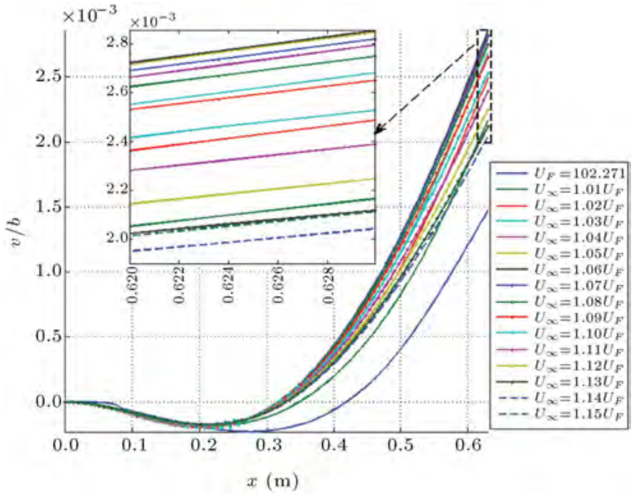

Figure 19. The lag static displacement along the span of the wing for different velocities at angle of attack 1 deg.

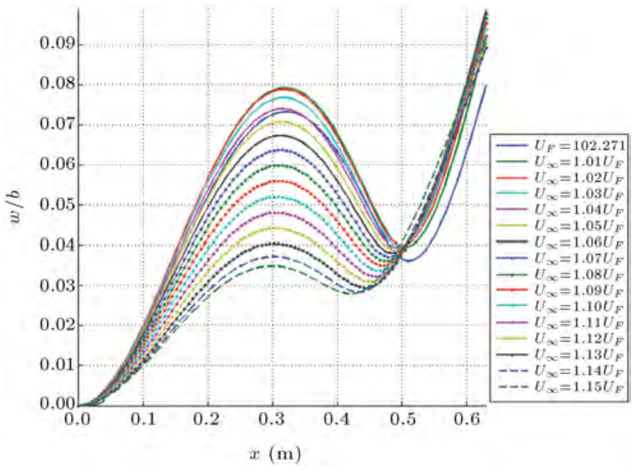

Figure 20. The flap displacement amplitude along the span of the wing for different velocities at angle of attack 5 deg.

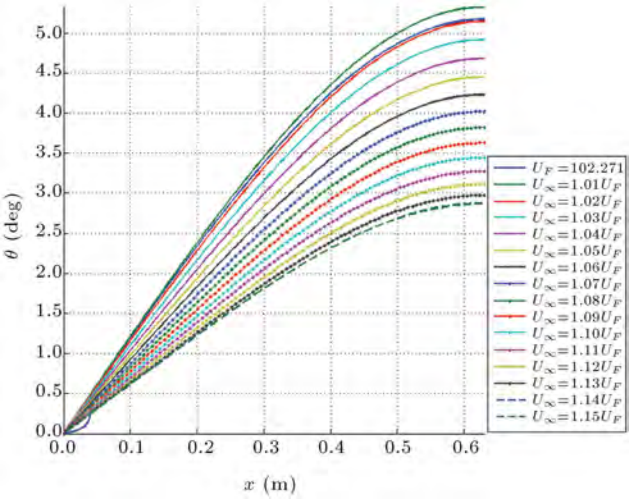

Figure 21. The torsion displacement amplitude along the span of the wing for different velocities at angle of attack 5 deg.

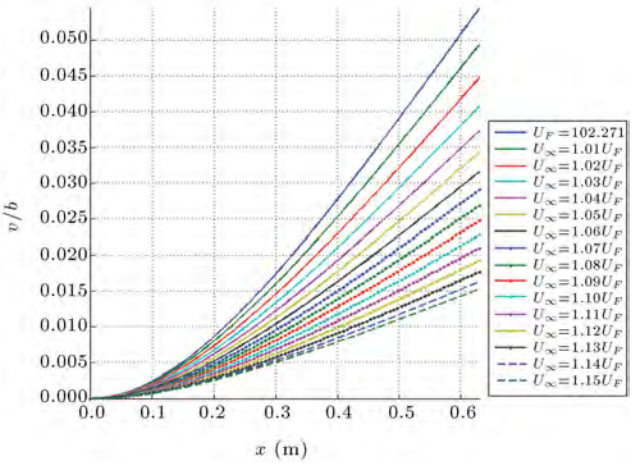

Figure 22. The lag displacement amplitude along the span of the wing for different velocities at angle of attack 5 deg.

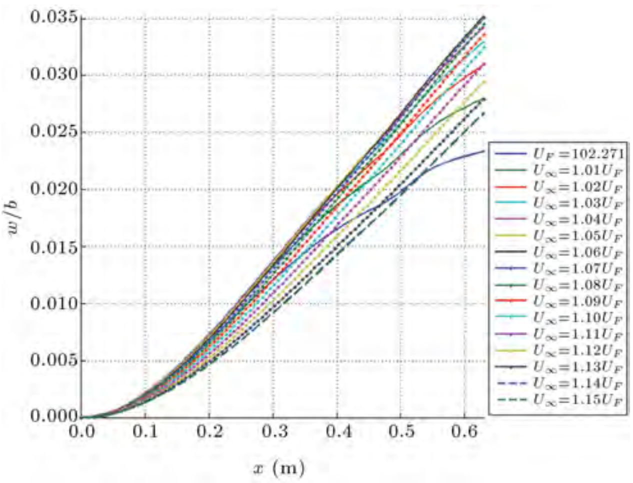

Figure 23. The flap static displacement along the span of the wing for different velocities at angle of attack 5 deg.

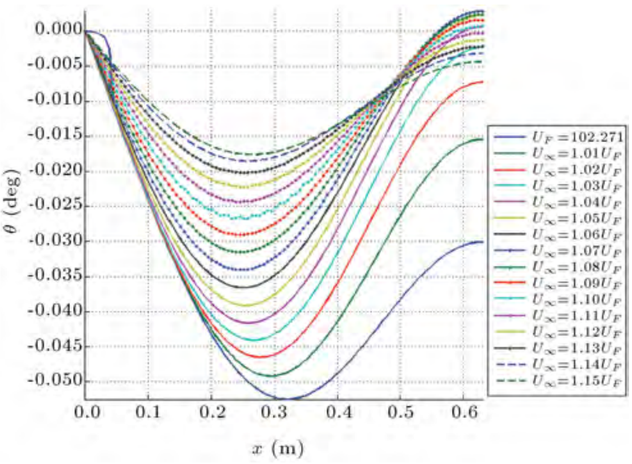

Figure 24. The torsion static displacement along the span of the wing for different velocities at angle of attack 5 deg.

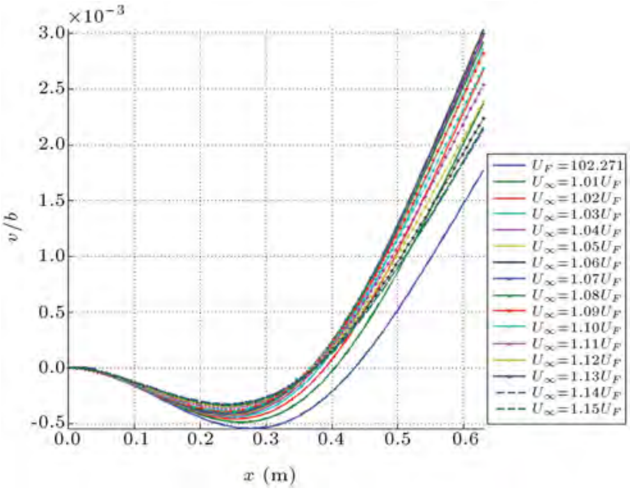

Figure 25. The lag static displacement along the span of the wing for different velocities at angle of attack 5 deg.

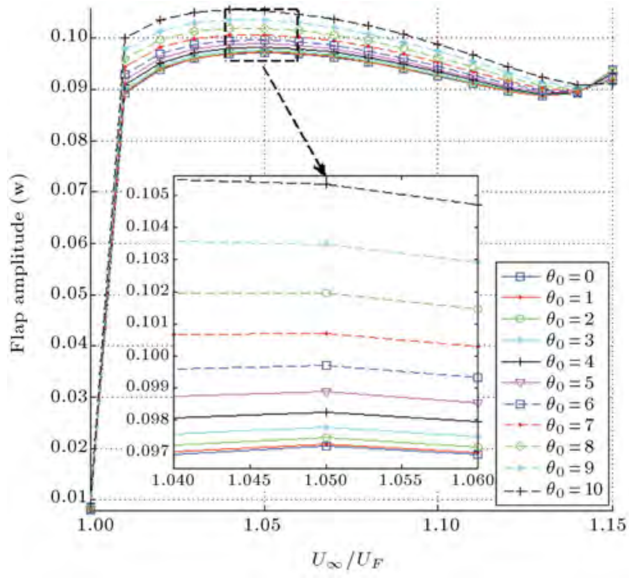

Figure 26. The flap displacement amplitude of the wing tip for different angle of attack.

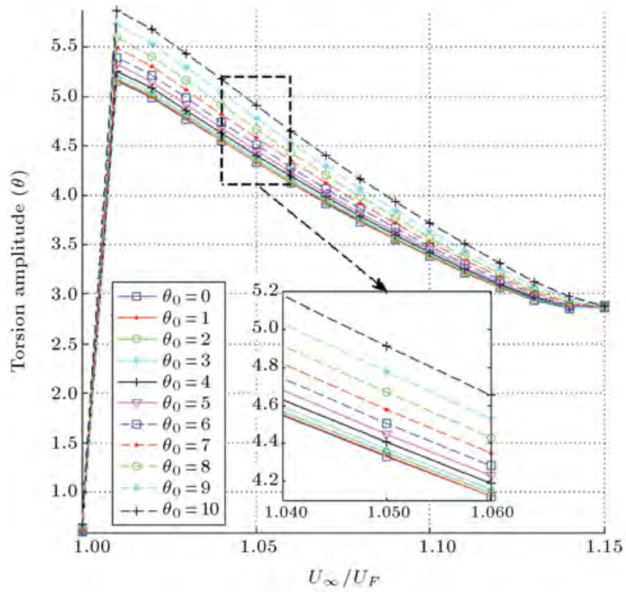

Figure 27. The torsion displacement amplitude of the wing tip for different angle of attack.

3.4. Effect of the attack angle on the limit cycle amplitude and frequency of nonlinear aeroelastic system

Now, the effect of the angle of the attack on limit cycle amplitudes will be examined. The flap, lag and torsion displacements at different velocities and different angles of attack are shown in Figures 26-28. According to these figures, by increasing the angle of attack from 0 to 10, lag amplitude increases gradually, while the changes of flap and torsion displacements are very small.

The variation of the flap static displacement with angle of attack is shown in Figure 29. According to this figure, by increasing angle of attack, the flap static amplitudes are increased by increasing free stream velocity. From these figures, it is clear that the amplitude of the oscillations in flutter velocity is very sensitive to the changes in the angle of attack.

The changes of the limit cycle oscillation frequency in different velocity and different angles of attack are shown in Figure 30. According to this figure, changes in angle of attack do not have any important effect on limit cycle frequency. The limit cycle frequencies decrease by increasing free stream velocity.

The wing tip cross section oscillations at the angle of attack of 1 deg are shown in Figure 31. According to Figure 31, in the extremum of motion, i.e., in the upper and lower part of the wing displacement, the main displacement is due to torsion, and sharp changes in the wing torsion occur. While between

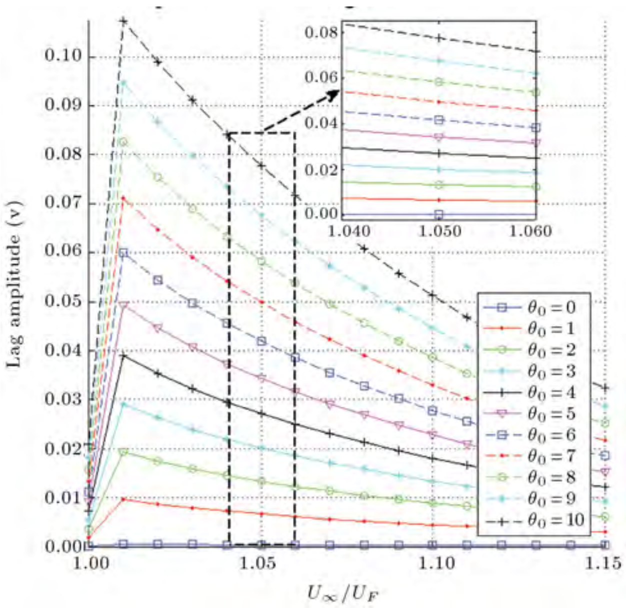

Figure 28. The lag displacement amplitude of the wing tip for different angle of attack.

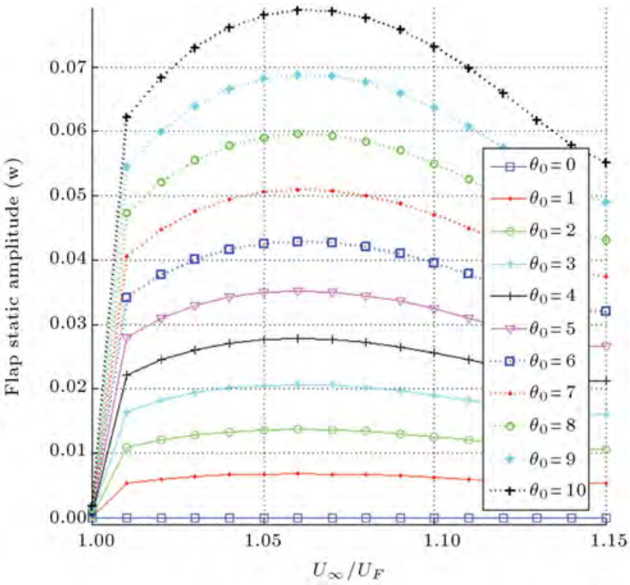

Figure 29. The flap static displacement amplitude of the wing tip for different angle of attack.

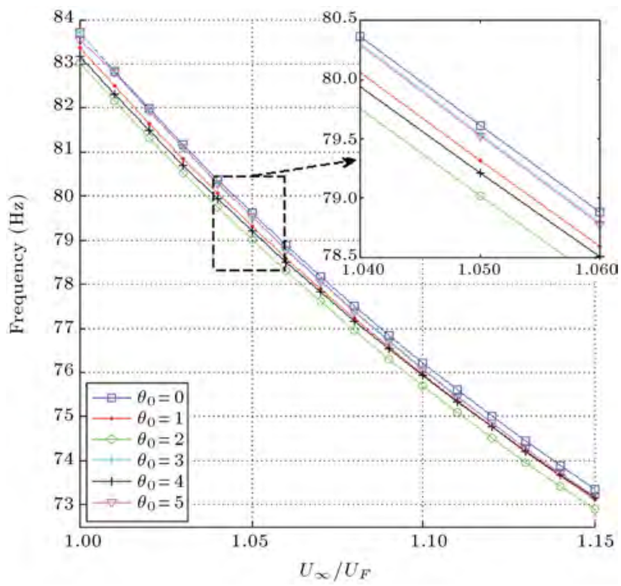

Figure 30. The frequency of the limit cycle oscillations at different angle of attacks.

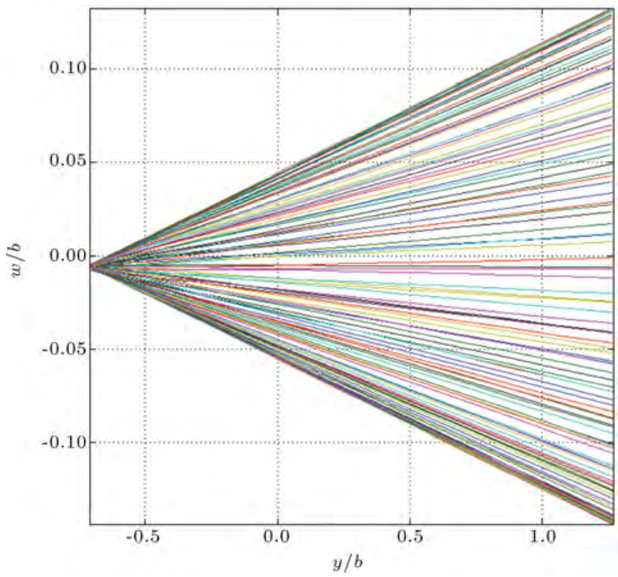

Figure 31. Wing cross section oscillations at position of 0.542 m at angle of attack 1 deg for velocity of 102.271 × 1.06 m/s.

these extrema, motion mainly due to bending displacements and torsion displacements gradually occurs.

Wing cross section oscillation at position has been shown in Figure 31. As seen from this figure, there is a node at the leading edge of the wing. The positions of this nodal line vary with free stream velocity and angle of attack.

4. Conclusion

In this study, the effect of the angle of attack on the nonlinear behavior of high aspect ratio wings in unsteady low speed aerodynamic flow is carefully examined. The studied wing models have flap, lag and torsion displacements. According to this study, the limit cycle amplitudes are very sensitive to variations in angle of attack. With variation of the angle of attack, wings undergo a static displacement in each displacement. The frequency of limit cycle oscillations at different angles of attack and free stream velocities is obtained. There are minor changes in the frequency of the limit cycle with variations in angle of attack.

Nomenclature

a_h	Dimensionless distance from wing section mid-chord to elastic axis
b	Wing section semi-chord
C_v, C_w	Structural chord-wise and vertical bending damping coefficents
C_θ	Structural twist damping
$c, \bar{c}$	Wing chord and dimensionless chord, c/L
dD, dL	Section drag and lift forces
dF_v, dF_w	Chord-wise and vertical aerodynamic forces
dM_x	Aerodynamic pitch moment about elastic axis
dM_{xf}	aerodynamic pitch moment about elastic axis
E	Modulus of elasticity of wing
e	Section mass center distance from elastic axis
G	Shear modulus of elasticity
h	Plunge displacement
I_1, I_2	Vertical, chord-wise area moments of inertia
J	Torsional stiffness constant
L	Wing span
m	Mass per unit length of the wing
r_α	Radius of gyration about elastic axis
t	Time
U, U^*	Free-stream velocity and dimensionless velocity
U_F	Flutter velocity
v_i, W_i	Generalized coordinates for flap lag bending
ν	Chord-wise or edgewise bending deflection
w	Vertical or flapwise bending deflection
x	Position coordinate along wing span
x_f	Position of flexural axis
x_α	Dimensionless distance from elastic axis to center of mass
θ	Pitch angle of wing section
θ_i	Generalized coordinates for torsion
θ_0	Steady angle of attack at root section
μ	Mass ratio
ζ, η	Dimensionless flap and lag displacements
ρ	Air density
τ	Dimensionless time
ω	Frequency of limit cycle oscillations
$\omega_\zeta, \omega_\eta, \omega_\alpha$	Natural frequencies in flap lag and pitch
ω_1^*, ω_2^*	Frequency ratio
$()'$	$d()/dx$
$(\dot{})$	d()/dt

References

1. Hodges, D.H. and Dowell, E.H. "Nonlinear equations of motion for the elastic bending and torsion of twisted non-uniform rotor blades", *NASA Technical note* (1974).
2. Tang, D. and Dowell, E.H. "Experimental and theoretical study on aeroelastic response of high-aspect-ratio wings",*AIAA Journal*, **39**(8), pp. 1430-1441 (2001).
3. Tang, D. and Dowell, E.H. "Experimental and theoretical study of gust response for high-aspect-ratio wing", *AIAA Journal*, **40**(3), pp. 419-429 (2002).
4. Patil, M.J., Hodges, D.H. and Cesnik, C.E.S. "Limit-cycle oscillations in high-aspect-ratio wings", *Journal of Fluids and Structures*, **15**(1), pp. 107-132 (2001).
5. Malatkar, P. "Nonlinear vibrations of cantilever beams and plates", PhD Dissertation, Virginia Polytechnic Institute and State University (2003).
6. Nichkawde, C. "Nonlinear aeroelastic analysis of high aspect ratio wings using the method of numerical continuation", Msc Dissertation, Texas, A& M University (2006).
7. Tang, D.M., Henry, J.K. and Dowell, E.H. "Effects of steady angle of attack on nonlinear gust response of a delta wing model", *Journal of Fluids and Structures*, **16**(8), pp. 1093-1110 (2002).
8. Gordnier, R.E. and Visbal, M.R. "Computation of the aeroelastic response of a flexible delta wing at high angles of attack", *Journal of Fluids and Structures*, **19**(6), pp. 785-800 (2004).
9. Tang, D.M. and Dowell, E.H. "Effects of angle of attack on nonlinear flutter of a delta wing", *AIAA Journal*, **39**, pp. 15-21 (2001).
10. Soltani, M.R., Ghorbanian, K. and Masdari, M. "Investigation of the pressure distribution and transition point over a swept wing", *Scientia Iranica, Transactions B: Mechanical Engineering* (2011), doi:10.1016/j.scient.2011.10.001.
11. Ghadimi, M., Dardel, M., Pashaei, M.H. and Barzegari, M.M. "Effects of geometric imperfections on the aeroelastic behavior of functionally graded wings in supersonic flow", *Aerospace Science and Technology*, **23**, pp. 492-504 (2012).
12. Davari, A.R., Soltani, M.R., Askari, F. and Pajuhande, H.R. "Effects of wing geometry on wing-body-tail interference in subsonic flow", *Scientia Iranica, Transactions B: Mechanical Engineering*, **18**, pp. 407-415 (2011).

13. Dardel, M. and Bakhtiari-nejad, F. "Limit cycle oscillation control of wing with static output feedback control method", *Aerospace Science and Technology*, **24**, pp. 147-160 (2013).

14. Jian, Z. and Jinwu, X. "Nonlinear aeroelastic response of high-aspect-ratio flexible wings", *Chinese Journal of Aeronautics*, **22**, pp. 355-363 (2009).

15. Qiang, W.Z., Hong, Y., Guang, L.D. and Chao, Y. "Aeroelastic analysis and optimization of high aspect ratio composite forward swept wings, *Chinese Journal of Aeronautics*, **18**(4), pp. 317-325 (2005).

16. Gordnier, R.E., Chimakurthi, S.K., Cesnik, C.E.S. and Attar, P.J. "High-fidelity aeroelastic computations of a flapping wing with span-wise flexibility", *Journal of Fluids and Structures*, **40**, pp. 86-104 (2013).

17. Xie, C., Wang, L., Yang, C. and Liu, Y. "Static aeroelastic analysis of very flexible wings based on non-planar vortex lattice method", *Chinese Journal of Aeronautics*, **26**(3), pp. 514-521 (2013).

18. Tang, D.M. and Dowell, E.H. "Effects of geometric structural nonlinearity on flutter and limit cycle oscillations of high-aspect-ratio wings", *Journal of Fluids and Structures*, **19**(3), pp. 291-306 (2004).

19. Fung, Y.C., *An Introduction to the Theory of Aeroelasticity*, John Wiley and Sons, Inc. (1995).

20. Lee, B.H.K., Liu, L. and Chung K.W. "Airfoil motion in subsonic flow with strong cubic nonlinear restoring forces", *Journal of Sound and Vibration*, **281**, pp. 699-717 (2005).

21. Ghadiri, B. and Razi, M. "Limit cycle oscillations of rectangular cantilever wings containing cubic nonlinearity in an incompressible flow", *Journal of Fluids and Structures*, **23**(4), pp. 665-680 (2007).

Appendix A.

Aeroelastic matrices coefficients:

$$M_{\zeta\zeta}^{ij} = \left(1 + \frac{1}{\mu}\right) \int_0^1 \psi_i \psi_j d\xi,$$

$$M_{\zeta\theta}^{ij} = \left(x_a - \frac{a_h}{\mu}\right) \int_0^1 \psi_i \phi_j d\xi,$$

$$M_{\zeta\eta}^{ij} = 0, \qquad M_{\theta\eta}^{ij} = 0,$$

$$M_{\theta\zeta}^{ij} = \left[\frac{x_a}{r_a^2} - \% \frac{a_h}{\mu r_a^2}\right] \int_0^1 \phi_i \psi_j d\xi,$$

$$M_{\theta\theta}^{ij} = \left(1 + \frac{1}{\mu r_a^2}\left(a_h^2 + \frac{1}{8}\right)\right) \int_0^1 \phi_i \phi_j d\xi,$$

$$M_{\theta\eta}^{ij} = 0, \qquad M_{\eta\zeta}^{ij} = -\frac{\theta_0}{\mu} \int_0^1 a_i \psi_j d\xi,$$

$$M_{\eta\theta}^{ij} = \frac{\theta_0 a_h}{\mu} \int_0^1 a_i \phi_j d\xi,$$

$$M_{\eta\eta}^{ij} = \int_0^1 a_i a_j dx,$$

$$C_{\zeta\zeta}^{ij} = \left(\frac{C_w}{m\omega_a U^*} + \frac{2\phi(0)}{\mu}\right) \int_0^1 \psi_i \psi_j d\xi,$$

$$C_{\zeta\theta}^{ij} = \frac{1 + (1 - 2a_h)\phi(0)}{\mu} \int_0^1 \psi_i \phi_j d\xi,$$

$$C_{\zeta\eta}^{ij} = 0, \quad C_{\theta\zeta}^{ij} = -\frac{(2a_h + 1)\phi(0)}{\mu r_a^2} \int_0^1 \phi_i \psi_j d\xi,$$

$$C_{\theta\theta}^{ij} = \left(\frac{C_\theta}{I_\theta \omega_a U^*} - \frac{(0.5 - a_h)\left[(1 + 2a_h)\phi(0) - 1\right]}{\mu r_a^2}\right) \times \int_0^1 \phi_i \phi_j d\xi,$$

$$C_{\theta\eta}^{ij} = 0, \quad C_{\eta\zeta}^{ij} = -\theta_0 \frac{2\phi(0)}{\mu} \int_0^1 a_j \psi_j d\xi,$$

$$C_{\eta\theta}^{ij} = -\frac{1 + (1 - 2a_h)\phi(0)}{\mu} \int_0^1 a_i \phi_j d\xi,$$

$$C_{\eta\eta}^{ij} = \frac{C_\nu}{m\omega_a U^*} \int_0^1 a_i a_j d\xi,$$

$$K_{\zeta\zeta}^{ij} = \left(\frac{-}{\frac{\omega}{U^*}}\right)^2 \frac{\int_0^1 \psi_1^2 dx^-}{\int_0^1 \left(\psi_1^{''}\right)^2 d\xi} \int_0^1 \psi_k^{''} \psi_i^{''} d\xi + \frac{2\phi(0)}{\mu} \int_0^1 \psi_k \psi_i d\xi,$$

$$K_{\zeta\theta}^{ki} = \frac{2(\phi(0) + (0.5 - a_h)\phi'(0))}{\mu} \int_0^1 \psi_k \phi_j d\xi,$$

$$K_{\zeta\eta}^{ki} = 0, \quad K_{\theta\zeta}^{ki} = -\frac{(2a_h + 1)\phi'(0)}{\mu r_a^2} \int_0^1 \phi_k \psi_j d\xi,$$

$$K_{\theta\theta}^{kj}=\sum_{j=1}^{N}\theta_j\left[\frac{1}{U^{*2}}\frac{\int_0^1\phi_1^2d\xi}{\int_0^1(\phi_1')^2d\xi}\int_0^1\phi_k'\phi_jd\xi\right.$$

$$\left.-\frac{(2a_h+1)[\phi(0)+(0.5-a_h)\phi'(0)]}{\mu r_a^2}\int_0^1\phi_k\phi_jd\xi\right],$$

$$K_{\theta\eta}^{kj}=0,\quad K_{\eta\zeta}^{kj}=\theta_0\frac{2\phi'(0)}{\mu}\int_0^1a_k\psi_id\xi,$$

$$K_{\eta\theta}^{ki}=\theta_0\frac{2(\phi(0)+(0.5-a_h)\phi'(0))}{\mu}\int_0^1a_k\phi_jd\xi,$$

$$K_{\eta\eta}^{ij}=\frac{\omega_2^{*2}}{U^{*2}}\frac{\int_0^1a_1^2dx}{\int_0^1a_1^{*2}dx}\int_0^1a_1^*a_j^*d\xi,$$

$$K_{\zeta1}^{ki}=\frac{2(\psi_1\epsilon_1[1-(0.5-a_h)\epsilon_1])}{\mu}\int_0^1\psi_k\phi_id\xi,$$

$$K_{\zeta2}^{ki}=\frac{2(\psi_2\epsilon_2[1-(0.5-a_h)\epsilon_2])}{\mu}\int_0^1\psi_k\phi_id\xi,$$

$$K_{\zeta3}^{ki}=-\frac{2\psi_1\epsilon_1^2}{\mu}\int_0^1\psi_k\psi_id\xi,\quad K_{\zeta4}^{ki}=-\frac{2\psi_2\epsilon\epsilon_2^2}{\mu}\int_0^1\psi_k\psi_id\xi,$$

$$K_{\theta1}^{kj}=-\frac{(2a_h+1)\psi_1\epsilon_1[1-(0.5-a_h)\epsilon_1]}{\mu r_a^2}\int_0^1\phi_k\phi_jd\xi,$$

$$K_{\theta3}^{ki}=\frac{(2a_h+1)\psi_1\epsilon_2^2}{\mu r_a^2}\int_0^1\phi_k\psi_id\xi,$$

$$K_{\theta2}^{ki}=-\frac{(2a_h+1)\psi_2\epsilon_1[1-(0.5-a_h)\epsilon_2]}{\mu r_a^2}\int_0^1\phi_k\phi_jd\xi,$$

$$K_{\theta4}^{ki}=\frac{(2a_h+1)\psi_2\epsilon_2^2}{\mu r_a^2}\int_0^1\phi_k\psi_id\xi,$$

$$K_{\eta1}^{ki}=\theta_0\frac{2(\psi_1\epsilon_1[1-(0.5-a_h)\epsilon_1])}{\mu}\int_0^1a_k\phi_id\xi,$$

$$K_{\eta2}^{ki}=\theta_0\frac{2\psi_2\epsilon_2[1-(0.5-a_h)\epsilon_2]}{\mu}\int_0^1a_k\phi_id\xi,$$

$$K_{\eta3}^{ki}=\theta_0\frac{2\psi_1\epsilon_1^2}{\mu}\int_0^1a_k\psi_id\xi,\quad K_{\eta4}^{ki}=-\theta_0\frac{2\psi_2\epsilon_2^2]}{\mu}\int_0^1a_k\psi_id\xi,$$

$$F_{N\zeta}=\left(\frac{EI_2}{EI_1}-1\right)\frac{\omega_1^{*2}}{U^{*2}}\frac{\int_0^1\psi_1^2d\xi}{\int_0^1\psi_1''^2d\xi}\sum_{j=1}^{N}\sum_{k=1}^{N}\eta_j\theta_k$$

$$\left(\int_0^1\psi_i'a_j''\phi_k'd\xi+\int_0^1\psi_i'a_j'''\phi_kd\xi\right)+\frac{(1-2a_h)\phi'(\tau)}{\mu}$$

$$\sum\theta_j(0)\int_0^1\psi_k\phi_jd\xi+\frac{2\phi'(\tau)}{\mu}\sum\zeta_i(0)\int_0^1\psi_k\psi_id\xi,$$

$$F_{N\theta}=-\left(\frac{EI_2}{EI_1}-1\right)\frac{\omega_1^{*2}}{r_a^2U^{*2}}\frac{\int_0^1\psi_1^2dx}{\int_0^1\psi_1''^2dx}$$

$$\sum_{j=1}^{N}\sum_{k=1}^{N}\zeta_j\eta_k\int_0^1\phi_i^0\psi_j''a_k''d\xi$$

$$-\frac{(0.5-2a_h^2)\phi'(\tau)}{\mu r_a^2}\sum\theta_j(0)\int_0^1\phi_k\phi_jd\xi$$

$$-\frac{(2a_h+1)\phi'(\tau)}{\mu r_1^2}\sum\zeta_i(0)\int_0^1\phi_k\psi_id\xi,$$

$$F_{N\eta}=\left(1-\frac{EI_1}{EI_2}\right)\frac{\omega_2^{*2}}{U^{*2}}\frac{\int_0^1a_1^2dx}{\int_0^1a_1^{*2}dx}$$

$$\sum_{j=1}^{N}\sum_{k=1}^{N}\zeta_j\theta_k\left(\int_0^1a_1'\psi_j''\phi_k'd\xi+\int_0^1a_1'\psi_j'''\phi_kd\xi\right)$$

$$+\theta_0\frac{(1-2a_h)\phi'(\tau)}{\mu}\sum\theta_j(0)\int_0^1a_k\phi_jd\xi$$

$$+\theta_0\frac{2\phi'(\tau)}{\mu}\sum\zeta_i(0)\int_0^1a_k\psi_id\xi.$$

Biographies

Morteza Dardel received a PhD degree in Solid Mechanics from Amirkabir University (Polytechnic of Tehran), Iran, in 2009, and is currently Assistant Professor in the faculty of Mechanical Engineering at Babol Noushirvani University of Technology, Iran.His research interests include aeroelasticity, nonlinear dynamics, vibration and control of continuous systems and smart structures.

Keivan Eskandary obtained BS and MS degrees in Engineering Mechanics from Mazandaran University, Iran, and is currently pursuing his academic career at Chamran University, Iran. His research interests include mechanical nonlinear vibrations and dynamics, thermo-elastic and viscoelastic laminate.

Mohammad Hadi Pashaei received a PhD degree from Surrey University, UK, in Space Structures, in 2004, and is currently Assistant Professor in the Faculty of Mechanical Engineering at Babol Noushirvani University of Technology, Iran. His research interests include structural dynamics, damping in structures and vibrational systems analysis.

Seyed Amir Hossein Kiaeian Moosavi received a MS degree from Babol University of Technology, Iran, in 2010, and is currently pursuing a PhD degree in Industrial and Information Engineering at the Department of Electrical, Mechanical and Managerial Engineering of the University of Udine. His research interests include dynamic modeling and vibration control of mechanisms with deformable members.